

Exotic Quantum States in HgTe Quantum Dots with Inverted Band Structures

Kai Chang* and W. K. Lou

SKLSM, Institute of Semiconductors, Chinese Academy of Sciences, P.O. Box 912, Beijing 100083, China

(Dated: September 11, 2019)

We investigate theoretically the electron states in HgTe quantum dots (QDs) with inverted band structures, i.e., a two-dimensional topological insulator. In sharp contrast to conventional semiconductor quantum dots, the quantum states in the gap of HgTe quantum dot with an inverted band structure are fully spin-polarized, and show ring-like density distributions near the boundary of the QD and spin-angular momentum locking, which is the consequence of the quantization of the edge states. The persistent charge currents and magnetic moments, i.e., the Aharonov-Bohm effect, can be observed in such QD structure and oscillate with increasing magnetic fields. This feature offers us a practical way to detect these exotic ring-like edge states using the SQUID technique.

PACS numbers: 73.21.La, 71.70.Ej, 71.70.Di, 73.23.Ra

The exponential growth in the power of computing and information processing is expected to encounter the quantum limit when the component size reaches the nanometer scale. Semiconductor quantum dots (QDs) have attracted intensive attention in the past decades due to its application in electronic devices [1, 2], e.g., single-electron transistors [3], light-emitting diodes [4], diode lasers [5] and solar cells [6]. The electron and hole ground states both localize at the central part of the QDs, which gives rise to a strong oscillator strength of the interband optical transition. This is the common feature for various semiconductor QDs with a positive bandgap, e.g., self-assembled InAs quantum dots grown by molecular beam epitaxy [7], GaAs quantum dots defined by lithographically patterned gate electrodes [8], or by well-developed etching technique [9]. Precise control of quantum states in QDs pave the way to realize highly desirable key functions in nano-electronics, quantum computing and quantum information processing.

ture and Γ_8 symmetry, while the top of the valence band shows a s -like feature and Γ_6 symmetry [10]. In this case, HgTe becomes insulating in the bulk with a gap separating the valence and conduction bands, but with gapless helical edge states that are topologically protected by the time reversal symmetry, named a topological insulator (TI) [11, 12]. This topological insulator, one of the recent remarkable discoveries, is a new state of quantum matter [11, 13–16]. The quantum spin Hall effect (QSHE) in such two-dimensional TIs was predicted theoretically [12] and observed experimentally [17]. Currently, the most works focus on searching for new TI materials [18] and novel transport properties [19–22]. However, the electron states in TI nanostructures, e.g., QDs, remains relatively unexplored. It is interesting to ask what kind of new quantum states emerge when the band structure of the QD is inverted by the spin-orbit interactions.

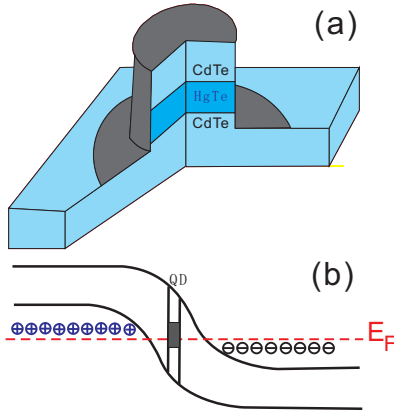


FIG. 1: (color online) (a) Schematic of a quantum dot formed in a HgTe heterostructure using etching technique. (b) Schematic of electrical injection of electrons and holes into a HgTe QD (the shaded region) embedded in a p-n junction.

By decreasing the bandgap, the band structure can be inverted. For instance, the bottom of the conduction band near the Γ point of the Brillouin zone in HgTe shows a p -like fea-

In this Letter we consider the quantum dots formed in HgTe heterostructure with an inverted band structure. Surprisingly, we find that the fully spin-polarized quantum states in the gap of the QD show a ring-like density distribution and spin-angular momentum locking, in sharp contrast to conventional semiconductor QDs where the electron is localized at the center of the QD. These states arise from the quantization of the edge states along the circumference of the QD, and its energies show a approximately linear dependence on the angular momentum. Importantly, these states are optical dark states that can be used in quantum information storage. A perpendicular magnetic field induces the persistent current and magnetic moment which oscillate with increasing magnetic fields, i.e., the Aharonov-Bohm (AB) effect. This fundamental quantum effect is never observed in a QD structure. This effect offer us a possibility for detecting these exotic states using the SQUID or STM techniques.

We consider a QD formed in a HgTe heterostructure using etching technique as shown schematically in Fig. 1. The low-energy electron states are described by a four band effective

Hamiltonian with a lateral confinement [12]:

$$H_{4 \times 4} = \begin{bmatrix} \varepsilon(k) + M(k) + V(\rho) & Ak_- & 0 & 0 \\ Ak_+ & \varepsilon(k) - M(k) - V(\rho) & 0 & 0 \\ 0 & 0 & \varepsilon(k) + M(k) + V(\rho) & -Ak_+ \\ 0 & 0 & -Ak_- & \varepsilon(k) - M(k) - V(\rho) \end{bmatrix} \quad (1)$$

where $\mathbf{k} = (k_x, k_y)$ is the in-plane momentum of carriers, $\varepsilon(k) = C - D(k_x^2 + k_y^2)$, $M(k) = M - B(k_x^2 + k_y^2)$, $k_{\pm} = k_x \pm ik_y$, and the parameters A, B, C, D, M depend on the thickness of HgTe quantum well. The Hamiltonian is obtained by reducing the eight-band Kane model to the reduced Hilbert space $|e \uparrow\rangle$, $|hh \uparrow\rangle$, $|e \downarrow\rangle$, and $|hh \downarrow\rangle$. Notice that the Hamiltonian is block-diagonal and possesses the time reversal symmetry for the upper and lower 2×2 blocks. M is an important parameter that can be used to describe the band insulator with a positive gap ($M > 0$) and topological insulator with a negative gap ($M < 0$) cases. The confining potential $V(\rho)$ of QD can be simulated by a hard-wall potential: $V(\rho) = 0$, for $\rho < R$; ∞ otherwise; R is the radius of the hard-wall disk. Other confining potentials, e.g., parabolic confinement, show the essentially same energy spectrum, we omit it here for the brevity [23]. The eigenstates and eigenenergies can be obtained numerically by expanding the wave function $\Psi_i = \sum_{n,\lambda} C_{n,\lambda}^{(i)} \varphi_{n,\lambda}$ in the terms of the Bessel basis for the hard-wall disk, where the index i corresponds to the different spin projection $S_z = \pm 1/2, \pm 3/2$. $C_{n,\lambda}^{(i)}$ is the expanding coefficient. For a hard-wall disk, the basis function $\varphi_{n,\lambda}$ can be expressed as $\varphi_{n,\lambda} = \mathbb{N}_C J_{\lambda}(k_n^{\lambda} \rho / R) e^{i\lambda\varphi}$, where k_n^{λ} is the n -th zero point of the first kind of the Cylinder Bessel functions $J_{\lambda}(x)$, $\mathbb{N}_C = 1 / [\sqrt{\pi} R J_{\lambda+1}(k_n^{\lambda})]$. $\lambda = 0, \pm 1, \pm 2, \dots$ is the quantum number of the angular momentum. Notice that λ is a good quantum number because the off-diagonal elements in the Hamiltonian (1) only couple the basis functions with the angular momenta $e^{i\lambda\varphi}$ and $e^{i(\lambda \pm 1)\varphi}$. In the presence of an external perpendicular magnetic field, the canonical momentum is $\mathbf{P} = \mathbf{p} + e\mathbf{A}$. $\mathbf{A} = \mathbf{B} \times \mathbf{r} / 2$ is the vector potential adopting the symmetric gauge. The number of the eigenstates used in the expansion is chosen to ensure the convergence of the calculated energies of the quantum states within and nearby the bulk gap.

We show the energy spectra of a HgTe QD with a hard-wall confining potential as a function of the angular momentum $m = \langle L_z \rangle$ in Fig. 2. The relevant parameters used in our calculation are obtained from Ref. [12]. In Fig. 2, we consider two different cases: the band insulator ($M > 0$) and the topological insulator ($M < 0$) cases. Comparing Fig. 2(a) with Fig. 2(b), one can see that the quantum dot spectrum is gapped for the band insulator QD case ($M > 0$), which is similar with that of the conventional semiconductor QDs. But for the topological insulator QD case ($M < 0$), the exotic quantum states emerge in the whole energy spectrum even in the gap. These states show a linear energy dispersion, i.e., the Dirac spectrum, against the angular momentum m in the bulk gap. The energy spectrum of these states (the red and blue

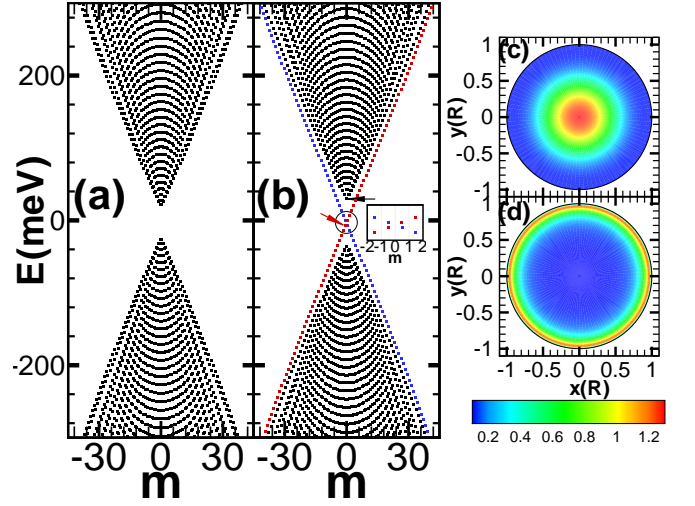


FIG. 2: (color online) The energy spectra of the HgTe QDs in band insulator ($M > 0$) and topological insulator ($M < 0$) cases as a function of the angular momentum m . (a) is in the band insulator phase ($M > 0$); (b) is in the topological insulator phase ($M < 0$). The new quantum states are denoted by the red (rotating clockwise) and blue (rotating counter-clockwise) squares. The inset is the amplification of the circle region near the Dirac point. (c) The density distributions of the lowest conduction band electron states [marked by the black arrow in Fig. 2(b)] in the QD; (d) The same as (c), but for the RES [marked by the red arrow in Fig. 2(b)] near the Dirac point. The QD radius $R = 55\text{nm}$, $M = -30\text{meV}$.

squares in Fig. 2(b)) shows symmetric respect to the angular momentum m due to the time reversal symmetry. In order to understand the physical origin of these states, we plot the density distribution of the quantum states appearing within the bulk gap in Figs. 2(c) and 2(d). Figure 2(c) shows the density distributions of the lowest conduction band electron states [marked by the black arrow in Fig. 2(b)], which peak at the center of the QDs as in conventional semiconductor quantum dots. Figure 2(d) describes the density distribution of the new quantum states [marked by the red arrow in Fig. 2(b)] nearby the Dirac point. Surprisingly, one can see the state localizes at the edge of the hard-wall QD, and shows the ring-like density distribution. We would stress that all these new quantum states carry approximately half-integer angular momentums $m = I \pm 1/2$, where the integer $I = 0, \pm 1, \pm 2, \dots$ [see the inset of Fig. 2(b)], and show the homocentric ring-like density distributions. We name these exotic quantum states as the ring-like edge states (RESSs) in this paper. We calculate the dependence of the energies of the bulk QD states and the RESSs on the size of the QD in Fig. 3(a). For the quantum states arising from the quantized electron bulk states localized at the center of the QD, the energy spectrum shows a linear dependence on the inverse of the area of the QD [see the inset of Fig. 3(a)], i.e., $1/R^2$. Interestingly, the energies of the RESSs display a perfect linear dependence on the inverse of the circumference of the QD, i.e., $1/R$. This feature indicates clearly that these exotic quantum states come from the quantization of the edge states in two-dimensional topological insulators along the circum-

ference of the hard-wall disk. The RESs are equally spaced in the energy spectrum [see Fig. 2(b)] because of the new quantization rule $m = I \pm 1/2$ and show the linear energy dispersion against the angular momentum m . This characteristic means that electrons in the RESs behave like massless Dirac fermions. When this massless Dirac fermion is confined in a disk, its lowest energy modes should be the whispering gallery mode, similar to a photon confined in a cylinder cavity. This gives us an intuitive picture to understand the origin of these exotic ring-like quantum states in QDs. From Fig. 3(b) one can see that the energy level spacing $\Delta E = E_m - E_{m-1}$ of the RESs (the gap of the bulk states $E_g = E_{m=0}^c - E_{m=0}^v$, the indexes c, v denote the conduction and valence bands, respectively) in the QD increase linearly as the inverse of the radius $1/R$ (area $1/R^2$) of the QD increases. It means that one can tune the energy level spacing ΔE significantly of the RESs by changing the QD size R .

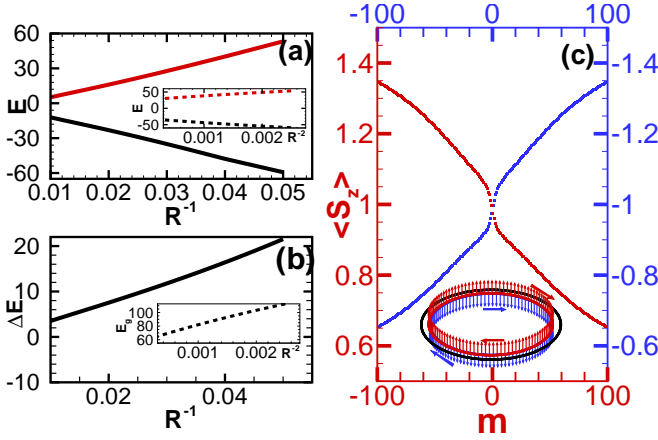


FIG. 3: (color online) (a) The energies of the up (the red line) and down (the black line) branches of the RESs vs the inverse of the radius of the QD $1/R$. The inset shows the dependence of the energies of the electron states in the bulk conduction (the red dashed line) and valence (the black dashed line) bands on the inverse square of the radius of the QD $1/R^2$, respectively. (b) The energy level spacing ΔE of the RESs vs the $1/R$, the inset shows the bulk energy gap of the QD vs $1/R^2$. (c) The spin projection $\langle S_z \rangle$ for the ring-like edge states with the different angular momentum m . The inset is the schematic of the spin orientation of the RESs in the QD. $R = 55\text{nm}$, $M = -30\text{meV}$.

Interestingly, these ring-like states are fully spin-polarized and show a spin-angular momentum locking. In Fig. 3(c), there are two kinds of these ring-like quantum states in which spin-up electrons rotate clockwise and spin-down electron rotate counterclockwise [see Fig. 3(c)]. This opposite spin orientation is the consequence of the time reversal symmetry in the four-band Hamiltonian (1). Note that the spin projection of edge states $\langle S_z \rangle$ is not a good quantum number, and varies significantly with increasing the angular momentum m . For the edge states rotating clockwise (the spin-up branch) and counterclockwise (the spin-down branch), the spin orientation $\langle S_z \rangle$ varies approximately from 0.6 to 1.4, and -0.6 to -1.4 , respectively, which indicates that the mixing between

the electron and the hole states changes with the angular momentum and therefore destroys the spin conservation. The spin orientation $\langle S_z \rangle$ is symmetric respect to the angular momentum $\langle m \rangle$, i.e., rotating clockwise and counterclockwise. Interestingly, this degeneracy $E_m = E_{-m}$ is lifted by a weak magnetic field, thus one can get a fully spin-polarized electron states by controlling the number of electrons in such a QD at low temperatures.

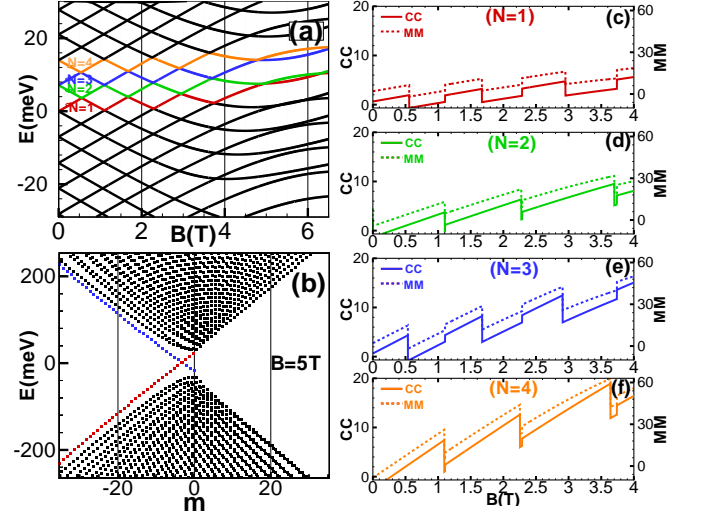


FIG. 4: (color online) (a) The magnetic level fan in a HgTe QD with a inverted band structure. (b) The energy spectrum in the presence of magnetic fields for the TI QD. (c)-(f) The persistent charge current (CC) (the solid line) and magnetic moment (MM) (the dashed line) in a TI QD against the magnetic fields for different electron number N . The persistent CC is in units of $2NE_0/\Phi_0$ ($2N * 2\pi A$ for the hard wall disk, where $E_0 = \hbar^2/[2m^*(R)^2]$. $R = 55\text{nm}$, $M = -30\text{meV}$. The magnetic moment is in units of $N\mu_B$, where $\mu_B = eh/(2m_e)$. The red, green, blue and orange curves indicates different electrons $N = 1, 2, 3, 4$ filled in the edge states (see the panel (a)).

Next we turn to discuss the optical property of these edge states in QDs. The absorption spectra of the QD $\alpha(\hbar\omega) = \frac{\pi e^2}{m_0^2 \epsilon_0 c n \omega V} \sum_{i,f} |\vec{\epsilon} \cdot \mathbf{P}_{if}|^2 \delta(E_f - E_i - \hbar\omega)$, where n is the refractive index, c is the speed of light in vacuum, ϵ_0 is the permittivity of vacuum, m_0 is the free-electron mass, and $\vec{\epsilon}$ is the polarization vector of the incident light. We are only interested in the vertical optical transition between the up and down branches of the edge states near the Dirac point, i.e., within in the bulk gap. The momentum matrix $\mathbf{P} \propto \partial H_{4 \times 4} / \partial \mathbf{k}$ is block diagonal and will not couple the up and down branches of the edge states belonging to the spin-up and spin-down families, therefore the vertical circular transition between the up and down branches is forbidden because of the conservation of the angular momentum. It makes it hardly possible to detect these ring-like edge states using optical techniques, e.g., photoluminescence. It means that these RESs are optically inactive within the electric dipole approximation, i.e., the dark states. However, the RESs also provides us a possibility to storage quantum information in these dark states, e.g., a electron-hole pair in the RESs formed by electric injection [see Fig. 1(b)].

Finally we study the effect of magnetic field on these RESs. We consider an external magnetic field applied perpendicularly to HgTe QD plane. Fig. 4(a) shows the magnetic levels in a HgTe QD ($M < 0$) including the bulk and edge states. The energy spectra display many crossing points in the bulk gap region. This is because an electron in these edge states shows a ring-like density distribution, and the energy spectrum is similar with that of a quantum ring. The energy spectra become no longer symmetric with respect to the angular momentum $< m >$ because the magnetic field breaks the time-reversal symmetry [see Fig. 4(b)]. The Dirac point is shifted left, and the edge states rotating clockwise (counterclockwise) is strongly squeezed (separated), since the Lorentz force induced by the magnetic field suppresses (enhances) electron rotating clockwise (counterclockwise). At high magnetic field ($R \gg l_B$), the edge states rotating clockwise are pushed into the bulk states and can not be seen in the spectra as shown in Fig. 4(b).

It is well known that a magnetic field can induce a persistent current in a mesoscopic ring, i.e., Aharonov-Bohm effect, which oscillates with increasing magnetic fields. Such quantum mechanical phenomenon is never observed in QD systems due to the topology of the QD geometric structure. Interestingly, this phenomenon can be found in this topological insulator QD system, because the unique density distributions of the RESs show a ring-like behavior and almost localized at the boundary of the hard-wall disk. The persistent current for a single TI QD can be obtained by $I = \int \hat{j}_c(r) d\vec{r}$, where the current density operator $\hat{j}_c(r) = [\hat{\rho}\hat{v} + \hat{v}\hat{\rho}]/2$, and the magnetic moment \vec{M} generated by the persistent current is given by: $\vec{M} = \int \vec{r} \times \hat{j}_c(r) d\vec{r}/2$, where $\hat{\rho}$ is the electron density operator, \hat{v} is the electron group velocity operator along the tangential direction [24]. From Figs. 4(c)-4(f), one can see that the magnitude of the magnetic moment induced by the persistent current depends on the electron numbers in the QD and ranges from $20 \sim 200\mu_B$, which is beyond the limit of resolution and sensitivity of near-field SQUID magnetometry (around $1 \sim 10\mu_B$) [25]. The persistent charge current and the magnetic moment are a periodic function of magnetic fields, exhibiting many linear segments with a fixed slope ratio. The periodicity of the persistent charge current for different electron number N is almost the same. This feature can be understood from the crossing points in the magnetic energy level spectrum in Fig. 4(a). When the magnetic field sweeps across the points, the persistent current and magnetic moment oscillate. The oscillation of the magnetic moment provides us a possibility to detect these exotic quantum states in HgTe QDs using near-field SQUID technique at low temperature [25, 26].

In summary, we study the exotic quantum states in quantum dots formed in HgTe heterostructure with inverted band structures. As a consequence of the quantization of the edge states, these states appear in the bulk gap of the QDs and show ring-like density distributions. The RESs are optically inactive since the vertical optical transition between these states is forbidden. This feature is in sharp contrast to that of the conventional semiconductor quantum dots with normal band

structures. The oscillating persistent currents and magnetic moments can be found as the perpendicular magnetic fields increase, which make it possible to detect these quantum states utilizing the nano-SQUID technique. This work shed a new light on constructing topological insulator-based nano-electronic devices.

This work was partly supported by the NSFC Grant Nos. 60525405 and 10874175, and the financial support from the MOST of China. KC would like to acknowledge Prof. S. C. Zhang for valuable discussions of the results.

* Electronic address: kchang@red.semi.ac.cn

- [1] D. Loss and D. P. DiVincenzo, Phys. Rev. A **57**, 120 (1998); A. Imamoglu, D. D. Awschalom, G. Burkard, D. P. DiVincenzo, D. Loss, M. Sherwin, and A. Small, Phys. Rev. Lett. **83**, 4204 (1999).
- [2] R. Hanson, L. P. Kouwenhoven, J. R. Petta, S. Tarucha, and L. M. K. Vandersypen, Rev. Mod. Phys. **79**, 1217 (2007).
- [3] M. A. Kastner, Rev. Mod. Phys. **64**, 849 (1992), and the references there in.
- [4] N. -M. Park, C. -J. Choi, T. -Y. Seong, and S. -J. Park, Phys. Rev. Lett. **86**, 1355 (2001).
- [5] S. Fafard, K. Hinzer, S. Raymond, M. Dion, J. McCaffrey, Y. Feng, S. Charbonneau, Science **274**, 1350 (1996).
- [6] A. Martí, E. Antolín, C. R. Stanley, C. D. Farmer, N. López, P. Díaz, E. Cánovas, P. G. Linares, and A. Luque, Phys. Rev. Lett. **97**, 247701 (2006).
- [7] M. Grundmann, J. Christen, N. N. Ledentsov, J. Böhrer, D. Bimberg, S. S. Ruvimov, P. Werner, U. Richter, U. Gösele, J. Heydenreich, V. M. Ustinov, A. Yu. Egorov, A. E. Zhukov, P. S. Kop'ev, and Zh. I. Alferov, Phys. Rev. Lett. **74**, 4043 (1995).
- [8] T. Hayashi, T. Fujisawa, H. D. Cheong, Y. H. Jeong, and Y. Hirayama, Phys. Rev. Lett. **91**, 226804 (2003).
- [9] L. P. Kouwenhoven, T. H. Oosterkamp, M. W. S. Danoesastro, M. Eto, D. G. Austing, T. Honda, S. Tarucha, Science **278**, 1788 (1997).
- [10] X. C. Zhang, A. Pfeuffer-Jeschke, K. Ortner, V. Hock, H. Buhmann, C. R. Becker, and G. Landwehr, Phys. Rev. B **63**, 245305 (2001).
- [11] C. L. Kane and E. J. Mele, Phys. Rev. Lett. **95**, 226801 (2005); *ibid.* **95**, 146802 (2005).
- [12] B. A. Bernevig, T. L. Hughes, and S. C. Zhang, Science **314**, 1757 (2006).
- [13] L. Fu and C. L. Kane, Phys. Rev. B **76**, 045302 (2007); J. C. Y. Teo, L. Fu, and C. L. Kane, *ibid.* **78**, 045426 (2008).
- [14] X. L. Qi, T. L. Hughes, and S. C. Zhang, Phys. Rev. B **78**, 195424 (2008).
- [15] X. L. Qi and S. C. Zhang, Phys. Today **63**, 33 (2010).
- [16] M. Z. Hasan and C. L. Kane, arXiv:cond-mat/1002.3895.
- [17] M. König, S. Wiedmann, C. Brüne, A. Roth, H. Buhmann, L. W. Molenkamp, X. L. Qi, and S. C. Zhang, Science **318**, 766 (2007).
- [18] H. J. Zhang, C. X. Liu, X. L. Qi, X. Dai, Z. Fang, and S. C. Zhang, Nature. Phys. **5**, 438 (2009). D. Hsieh, D. Qian, L. Wray, Y. Xia, Y. S. Hor, R. J. Cava, and M. Z. Hasan, Nature (London) **452**, 970 (2008). H. Lin, R. S. Markiewicz, L. A. Wray, L. Fu, M. Z. Hasan, and A. Bansil, Phys. Rev. Lett. **105**, 036404 (2010).
- [19] D. Hsieh, Y. Xia, D. Qian, L. Wray, J. H. Dil, F. Meier, J. Oster-

- walder, L. Patthey, J. G. Checkelsky, N. P. Ong, A. V. Fedorov, H. Lin, A. Bansil, D. Grauer, Y. S. Hor, R. J. Cava, and M. Z. Hasan, *Nature (London)* **460**, 1101(2009).
- [20] W. Yang, Kai Chang, and S. C. Zhang, *Phys. Rev. Lett.* **100**, 056602 (2008).
- [21] B. Zhou, H. Z. Lu, R. L. Chu, S. Q. Shen, and Q. Niu, *Phys. Rev. Lett.* **101**, 246807 (2008).
- [22] E. B. Sonin, arXiv:cond-mat/1006.5218.
- [23] In order to investigate the influence of the confining potential on the energy spectrum, we have also considered the parabolic confining potential $V(\rho) = K\rho^2/2$, where $K = m^*\omega_0^2$. In this parabolic QD case, the wave function is expanded in the terms of the Fock-Darwin basis $\varphi_{nm} = \mathbb{N}_p e^{-\rho^2/2} (\rho/l_\Omega)^{|m|} L_n^{|m|} (\rho^2/l_\Omega^2) e^{im\varphi}$, where the $L_n^{|m|}(x)$ is the Laguerre function, $l_\Omega = (\hbar/m^*\Omega)^{1/2}$, $\Omega = \sqrt{\omega_0^2 + (\omega_c/2)^2}$, $\omega_c = eB/m^*$, $\mathbb{N}_p = [n!/\pi(n+|m|)!]^{1/2}/l_\Omega$. The calculation results in the parabolic QD is the same as that for the hard-wall disk, which indicates the ring like edge states are independent of confining potential. For brevity we only show the results of a cylinder hard-wall disk in this paper.
- [24] J. S. Sheng and Kai Chang, *Phys. Rev. B* **74**, 235315 (2006).
- [25] V. Bouchiat, *Supercond. Sci. Technol.* **22** 064002 (2009).
- [26] W. Rabaud, L. Saminadayar, D. Mailly, K. Hasselbach, A. Benoît, and B. Etienne, *Phys. Rev. Lett.* **86**, 3124 (2001).